Tetrahedron 67 (2011) 303–311

Contents lists available at ScienceDirect

Tetrahedron

journal homepage: www.elsevier.com/locate/tet

Synthesis and applications of novel acceptor–donor–acceptor organic dyes with dithienopyrrole- and fluorene-cores for dye-sensitized solar cells

Duryodhan Sahu [a], Harihara Padhy [a], Dhananjaya Patra [a], Jen-Fu Yin [a], Ying-Chan Hsu [b], Jiann-T'Suen Lin [b], Kuang-Lieh Lu [b], Kung-Hwa Wei [a], Hong-Cheu Lin [a,*]

[a] Department of Materials Science and Engineering, National Chiao Tung University, Hsinchu, Taiwan, ROC
[b] Institute of Chemistry, Academia Sinica, Taipei 115, Taiwan, ROC

ARTICLE INFO

Article history:
Received 21 September 2010
Received in revised form 2 November 2010
Accepted 9 November 2010
Available online 13 November 2010

Keywords:
Dye-sensitized solar cell
Di-anchoring dyes
Acceptor–donor–acceptor
Density function theory
Electron lifetime

ABSTRACT

Four novel symmetrical organic dyes (**S1**–**S4**) configured with acceptor–donor–acceptor (A–D–A) structures containing electron donating fluorene (**S1** and **S2**) and *N*-alkyl dithieno[3,2-*b*:2′,3′-*d*]pyrrole (DTP) (**S3** and **S4**) cores terminated with two anchoring cyanoacrylic acids (as electron acceptors) were synthesized and applied to dye-sensitized solar cells (DSSCs). The DSSC device based on **S2** dye showed the best photovoltaic performance among **S1**–**S4** dyes: a maximum monochromatic incident photon-to-current conversion efficiency (IPCE) of 76%, a short circuit current (J_{SC}) of 12.27 mA/cm^2, an open circuit voltage (V_{OC}) of 0.61 V, a fill factor (FF) of 0.63, and an overall power conversion efficiency (η) of 4.73%. Besides, the utilization of chenodoxycholic acid (CDCA) as a co-adsorbent in the DSSC device based on **S3** dye showed a significant improvement in its η value (from 3.70% to 4.31%), which is attributed to the suppression of dye aggregation on TiO_2 surface and thus to increase the J_{SC} value eventually.

1. Introduction

The growing global energy demands attracted significant attention to develop renewable energy resources. As a renewable source of energy, DSSCs became one of the most promising low cost alternatives to conventional photovoltaics.[1] After the successful exploration by Michael Grätzel,[2,3] DSSCs based on Ru-photosensitizers, such as N3 and N719, have been extensively investigated and developed.[4,5] So far, the Ru sensitizers have been reported with impressive solar-to-electrical power conversion efficiency values of ~11%.[4–9] However, in addition to high cost of rare Ru metal, the ruthenium dyes featuring relatively low molar extinction coefficients and tedious purification processes,[5] made scientists to think and develop the metal-free organic sensitizers lately. In contrast to those metal sensitizers, to reach higher efficiencies of metal-free sensitizers remained a challenge and a great progress has been made in this field hitherto. Various metal-free organic dyes, such as coumarin,[10] indoline,[11,12] cyanine,[13,14] merocyanine,[15] perylene,[16] thiophene,[17] and fluorene,[18–20] have been reported as efficient sensitizers for DSSCs, where the higher molar extinction coefficients of metal-free organic dyes enhanced the net light harvesting.

There are numerous dyes with common structural compositions, i.e., an electron donor with a high absorption band in the visible range and an electron acceptor (most notably cyanoacrylic acid), which facilitate vectorial charge transfers upon light absorption as well as assist the dye to anchor on the TiO_2 surface, and a π-conjugated spacer between the donor and acceptor has been reported to enhance the charge carrier mobilities with effective intramolecular charge transfers.[21]

However, researches on DSSC have led to a greater understanding of the key dye characteristics like, possessing high molar extinction coefficients[18,19] low band gaps and capable of absorbing the entire solar spectrum that make dyes to achieve high power conversion efficiencies.[22–24] Most importantly, the structural configurations of dyes that containing multiple electron acceptors followed by anchoring groups can generate photoinduced intramolecular charge transfer (ICT), which can inject electrons to the TiO_2 conduction band.[14,15,25–27] Due to the efficient light harvesting and high molar extinction coefficients, fluorene-based compounds exhibited some significant power conversion efficiencies both in DSSC and polymer solar cell applications.[18,19] Rasmussen and co-workers pioneered the use of *N*-alkyl dithieno[3,2-*b*:2′,3′-*d*]pyrrole (DTP) as a promising fused aromatic building block for electronic materials.[28] Since then, the introduction of DTP units imparted enhanced conjugation, high conductivity, and high charge carrier mobility for electronic materials, such as organic light-emitting diodes (OLEDs),[29] organic photovoltaic devices (OPVs),[30] and field effect transistors (FETs).[31]

* Corresponding author. Tel.: +886 3 5712121x55305; fax: +886 3 5724727; e-mail address: linhc@mail.nctu.edu.tw (H.-C. Lin).

0040-4020/$ – see front matter © 2010 Elsevier Ltd. All rights reserved.
doi:10.1016/j.tet.2010.11.044

However, no attention has been paid to use this novel high conjugated aromatic (DTP) unit in DSSC researches since its structural invention. There are still some major drawbacks for organic dyes used in DSSCs, such as the dye aggregations, poor electron lifetime and high charge recombination that hinder efficient injections of the excited dyes to the conduction bands so as to decrease the overall performances.[23,32–34] As a result, many efforts of using co-adsorbents and engineering molecular structures,[10a,22a,23] have been made to overcome those problems and to enhance their power conversion efficiencies.

As shown in Fig. 1, four acceptor–donor–acceptor (A–D–A) configured dyes with two different donors (fluorene and DTP cores) were designed as follows: (1) Fluorene: it enhanced the net molar extinction coefficient with different thiophene spacers[17–19] (2 and 3 thiophene units in **S1** and **S2**, respectively); (2) DTP: a new (in the field of DSSC application) fused aromatic building block, enhanced absorption spectra with various thiophene spacers (1 and 2 thiophene units in **S3** and **S4**, respectively). The di-hexyl and branched octyl side-chains in fluorene (**S1**–**S2**) and DTP (**S3**–**S4**) cores, respectively, increased the solubility and steric hindrance of the dianchoring dyes to adsorb on TiO_2 surfaces. The use of conducting thiophene spacers and cyanoacrylic acid termini (electron acceptors) in **S1**–**S4** dyes gave higher absorption spectra and thus to enhance their photovoltaic parameters crucially.[20,25] Furthermore, to provide a clear substantiation of the electronic structures and optical properties, we performed density functional theory/time-dependent density function theory (DFT/TDDFT) through optimization and calculation of their delocalizations in HOMO/LUMO levels. Compared with DTP-based **S3**–**S4** dyes, the DSSC containing fluorene-based **S2** dye achieved the highest power conversion efficiency (PCE) value (η=4.83%), which was attributed to its high molar extinction coefficient (11.9×10^4 M^{-1} cm^{-1} at 484 nm),[19,22] though it has a shorter absorption wavelength. The predicted broader spectral response of **S4** dye was not decisive for the photovoltaic performance due to its shorter electron lifetime induced by the oxidized dye, which accelerated the recombination of electrons in TiO_2 surface with redox species yielding lower photocurrent. Moreover, chenodoxycholic acid (CDCA) as co-adsorbent was used in the sensitization processes of **S2** and **S3** dyes in order to overcome the negative effects of dye aggregations on TiO_2 surfaces and enhance the η values.[22a,23] As a result, the overall PCE value of **S3** was improved significantly (η value increased from 3.70 to 4.31%), regardless to the negligible change in **S2** dye.

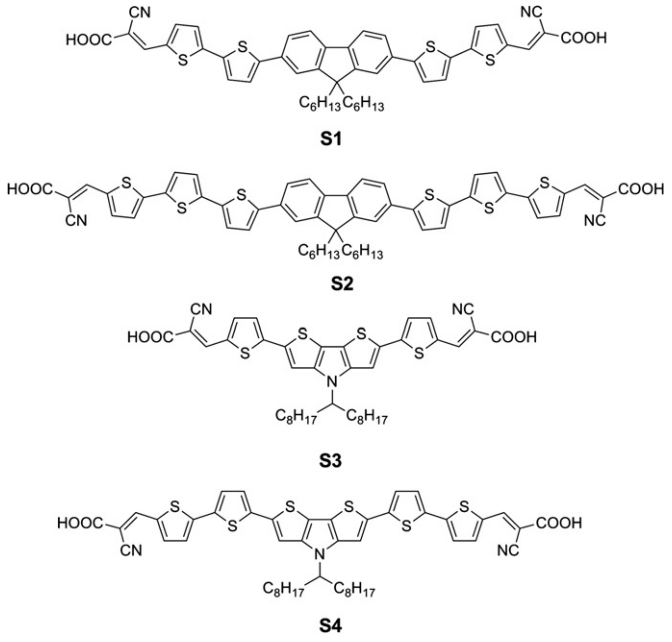

Fig. 1. Molecular structures of organic dyes (**S1**–**S4**).

2. Results and discussion

2.1. Optical properties

The UV–vis absorption and normalized photoluminescence (PL) spectra of dyes in THF solutions are displayed in Fig. 2a and b, respectively, and their corresponding data are listed in Table 1. As shown in Table 1, both molar extinction coefficients of **S1** (ε=9.20×10^4 M^{-1} cm^{-1}) and **S2** (ε=11.19×10^4 M^{-1} cm^{-1}) at their correspondent absorption maxima are higher than those of **S3** (ε=7.46×10^4 M^{-1} cm^{-1}) and **S4** (ε=7.90×10^4 M^{-1} cm^{-1}), which can be attributed to the fused phenyl rings of fluorene cores[18] in **S1** and **S2** dyes instead of the fused thiophene rings of *N*-alkyl dithieno [3,2-*b*:2′,3′-*d*]pyrrole (DTP) cores[35] in **S3** and **S4** dyes. These higher molar extinction coefficients indicate, **S1** and **S2** dyes bearing fluorene cores have facilitated higher light harvesting efficiencies than **S3** and **S4** dyes containing DTP cores. By adding one more thiophene unit on both sides of conjugated spacers in the symmetrical acceptor–donor–acceptor (A–D–A) structures, the increases of conjugation lengths from **S1** to **S2** and from **S3** to **S4** enhanced the molar extinction coefficients, respectively. Hence, **S2** dye with the largest molar extinction coefficient has the highest light harvesting efficiency, which subsequently promotes **S2** to have the best photovoltaic performance among all dyes (**S1**–**S4**). Except **S4** (with

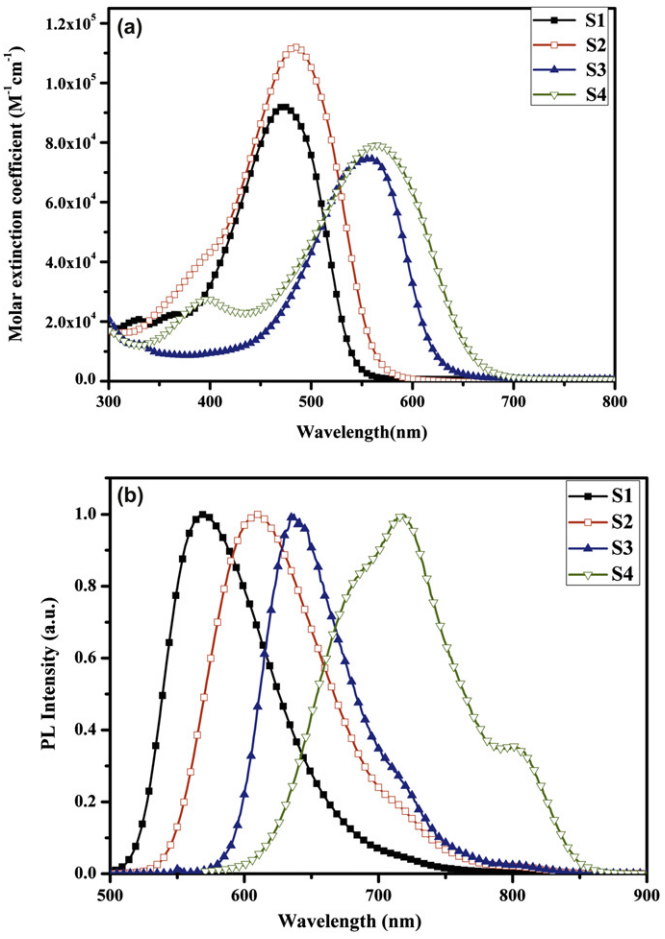

Fig. 2. (a) UV–vis absorption, (b) Normalized PL spectra, of **S1**–**S4** dyes (excited at 480 and 560 nm, respectively) recorded in THF solutions (concentration at 1.0×10^{-5} M).

Table 1
Electro-optical parameters of dyes (**S1**–**S4**)

Dye	λ_{max}/nm ($\varepsilon\times10^4$, M^{-1} cm^{-1})[a]	λ_{max} on TiO_2 (nm)[b]	λ_{em} (nm)[a]	Eg^{opt} (eV)[c]	HOMO/LUMO (eV)[d]	Stokes Shift (nm)[e]
S1	473 (9.20)	441	568	2.23	−5.58/−3.35	95
S2	484 (11.19)	457	610	2.14	−5.47/−3.33	126
S3	557 (7.46)	508	637	1.92	−5.32/−3.40	80
S4	395 (2.74), 564(7.90)	510	718	1.80	−5.14/−3.34	154

[a] Absorption and PL emission wavelength measured in THF solution (10^{-5} M).
[b] Absorption spectra of the dyes on 1.5 μm TiO_2 film.
[c] Optical band gap calculated from absorption onset ($Eg^{opt}=1240/\lambda_{edge}$).
[d] HOMO=[−(E_{onset}−0.45)−4.8] eV where 0.45 V is the value for ferrocene versus Ag/Ag^+ and 4.8 eV is the energy level of ferrocene below the vacuum, and LUMO of the dyes calculated by subtraction of the optical band gap from the HOMO.
[e] Stokes shift has been calculated from the difference between λ_{max} and λ_{em}.

a weak π−π* transition band at 395 nm and a prominent ICT band at 564 nm), **S1**–**S3** dyes have a single intense band at 473, 484, and 557 nm, respectively, representing the superpositions of π−π* and ICT transitions (see Table 1). An elongation of the π-conjugation caused a smaller π−π* energy gap and a spectral red shift for the π−π* transition was expected. Thus, bathochromic shifts from **S1** to **S2** (11 nm) and **S3** to **S4** (7 nm) were observed as a result of extended π-conjugations. Similar to the molar extinction coefficients, the maximum wavelengths (λ_{max}) of UV−vis absorption spectra increase as the conjugation lengths enlarged from **S1** to **S2** and from **S3** to **S4** by inserting more thiophene units on both symmetrical spacers,[36] which is consistent with the theoretical computational data (see Fig. 3b). In addition, owing to the higher effective conjugation lengths of **S3**–**S4** dyes containing *N*-alkyl dithieno[3,2-*b*:2′,3′-*d*]pyrrole (DTP) cores, their absorption spectra shifted to higher wavelength than those of fluorene containing **S1**–**S2** dyes. Fig. 3a shows the absorption spectra of the organic dyes (**S1**–**S4**) on TiO_2 films with a thickness of 1.5 μm and the data are illustrated in Table 1. Compared with the absorption spectra in solutions, the blue-shifted absorption (λ_{max}) wavelengths on TiO_2 surfaces were ascribed to the deprotonation of carboxylic acid present in the dyes.[37] However, the spectra of the dyes were distinctly broadened to longer wavelengths and such a broadening of the absorption spectra is attributable to an interaction between the dyes and TiO_2 surfaces. In PL spectra, where **S1**–**S2** excited at 480 nm and, **S3**–**S4** at 560 nm, showed a weak emission with stokes shift in the range 80–154 nm.

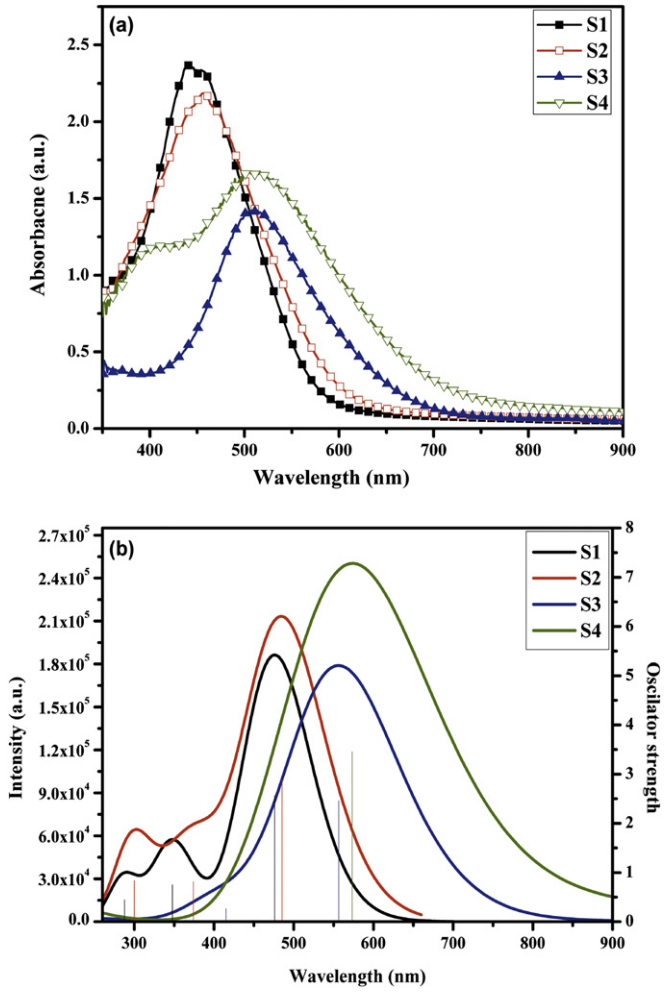

Fig. 3. (a) Absorption spectra of dyes adsorbed on 1.5 μm TiO_2 film, (b) Theoretical calculation of absorption spectra and oscillation strengths using B3LYP/6-31G*.

2.2. Electrochemical properties

The cyclic voltammetry (CV) measurements were performed in THF solutions to investigate the possibilities of electron transfer from the excited states of **S1**–**S4** dyes to the conduction bands of TiO_2 along with the dye charge regenerations, which correspond to the HOMO and LUMO levels of the organic dyes (**S1**–**S4**), and the CV results are illustrated in Table 1. Owing to the presence of central electron donating moieties (Fluorene or DTP), all dyes showed a quasi reversible oxidation potential (Fig. 4). The HOMO levels of the dyes were in the range −5.58 to −5.14 eV with respect to I^-/I_3^- redox couple (−4.60 eV vs vacuum), thus the low energy levels of dyes ensured negative Gibb's energies and thus provided enough driving forces for the charge regenerations.[23,38] However, comparably the high energy level (−5.14 eV), i.e., the low oxidation potential, of **S4** dye hindered its effective charge regeneration and recaptured the injected electrons by the dye cation radical.[37] The deduced LUMO levels were in the range of ca. −3.33 to −3.6 eV, which are higher than the conduction band edge (−4.0 eV vs vacuum), thus indicating that the electron injection process is energetically favorable. To gain an insight into the electronic states of these dyes, a DFT calculation has been performed using B3LYP hybrid functional and 6-31G* basis sets. As shown in Fig. S1 of the Supplementary data, the HOMO levels of **S1** and **S2** dyes are mainly delocalized on the central electron donating moieties (Fluorene) and the LUMO levels are on the cyanoacrylic acid anchoring units. In addition, there were overlappings of both HOMO and LUMO levels in the π-bridged thiophene units. According to Franck condon principle, these overlappings of both HOMO and LUMO levels in the π-bridged thiophene units enhance the electronic transition dipole moments between vibrational energy levels.[39] In general, it revealed that the HOMO to LUMO excitations moved the electron density distribution from central electron donating units (Fluorene) to the terminal cyanoacrylic acids efficiently. Nevertheless, in **S3** and **S4** dyes, the HOMO levels were entirely populated on DTP moiety and LUMOs on the cyanoacrylic acid anchoring units as well as on the donating moieties. Hence, the encumbrances in the electronic transitions between the vibrational energy levels had been anticipated in **S3** and **S4** dyes.

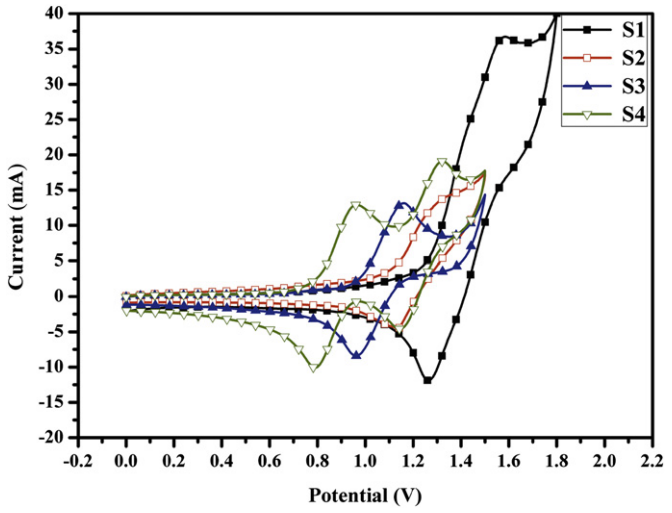

Fig. 4. Cyclic voltammograms of dyes in deoxygenated THF containing 0.1 M $TBAPF_6$ at room temperature. All potentials are in volts versus $Ag/AgNO_3$ at a scan rate of 100 mV/s.

2.3. Photovoltaic properties of DSSCs

The photovoltaic properties of DSSCs containing **S1**–**S4** dyes were measured under simulated AM 1.5 irradiation condition (100 mW/cm^2), where TiO_2 photoelectrodes with approximately a thickness of 18 μm and a working area of 0.25 cm^2 were utilized. The incident photon-to-current conversion efficiency (IPCE) and photocurrent–voltage (J–V) curves of DSSCs based on **S1**–**S4** and N719 dyes are shown in Figs. 5 and 6, respectively, and the details of photovoltaic parameters, such as the open-circuit photovoltage (V_{OC}), short-circuit photocurrent density (J_{SC}), fill factor (FF), and solar-to-electrical energy conversion efficiency (η) are listed in Table 2. The fluorene-based **S2** exhibited the best energy conversion efficiencies (η=4.73%) among **S1**–**S4** dyes, with V_{OC}=0.61 V, J_{SC}=12.27 mA/cm^2, and FF=0.63 (see Table 2). As described previously, due to the largest molar extinction coefficient, **S2** dye had the highest light harvesting efficiency and consequently promoted **S2** to have the best photovoltaic performance among all dyes (**S1**–**S4**). As shown in Fig. 5, the IPCE spectra of **S2** showed a broader response in the range of 300–700 nm and the maximum value exhibited a strikingly high plateau at 76%. Owing to the presence of highly conjugated electron-donating DTP moieties in **S3** and **S4** dyes, they showed broader (extended up to 800 nm) but much smaller maximum values of IPCE spectra than the fluorine-based **S1** and **S2** dyes. The decreased IPCE values suggest that there are poor injections of electrons from excited dyes to the TiO_2 conduction bands. In contrast to **S1** dye, the IPCE values of **S2** were enhanced by the longer conjugated thiophene linkers. On the contrary, compared with **S3** dye, **S4** possessed much smaller IPCE values is attributed to the highest HOMO level of **S4** dye (see Table 1), which led to a slower regeneration of the oxidized dye and higher recombination of photoinjected electrons.[33] Furthermore, the increase of **S4** dye aggregations on TiO_2 surface decreased the IPCE values significantly (see Fig. 5) though it has the highest absorption wavelength.[37] The higher molar extinction coefficient and oscillator strength of **S2** than **S1** reflected to an enhanced light harvesting in **S2** dye, and accordingly an improved J_{SC} (12.27 mA/cm^2) value was observed. Conversely, compared with **S3** dye, there were dramatic falls in both J_{SC} and V_{OC} values of **S4** (though the molar extinction coefficient and oscillator strength of **S4** were higher than those of **S3**). As a consequence, higher aggregations of **S4** than **S3** on TiO_2 surfaces caused the barrier in efficient electron injections from the excited dye to the conduction band of TiO_2 and comparably the shorter lifetime of oxidized **S4** dye caused a fast charge recombination process at the titinia/dye/electrolyte interface of **S4** dye.[32] Despite of both lower molar extinction coefficient and IPCE values of **S3** (in contrast to **S1**), it showed a higher η value, which could be attributed to the red shift of the maximum absorption wavelength (λ_{max}), the wider absorption spectra, and partly ascribed to the broadening of IPCE spectra towards a longer wavelength region.

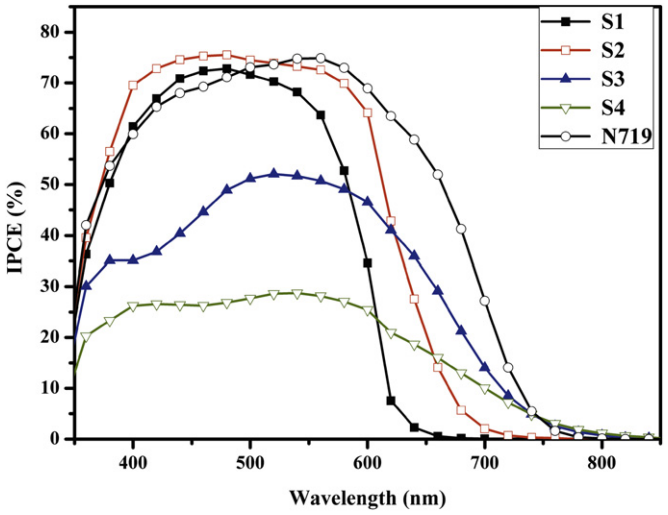

Fig. 5. IPCE plots for the DSSCs based on the organic dyes (**S1**–**S4** and N719).

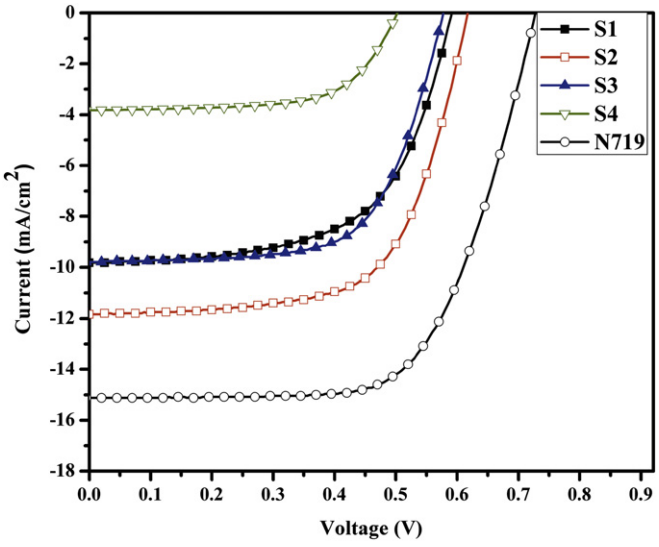

Fig. 6. J–V curves of DSSCs based on the organic dyes (**S1**–**S4** and N719) under illumination of simulated solar light (AM 1.5, 100 mW/cm^2). The electrode used was 0.5 M lithium iodide (LiI), 0.05 M iodine (I_2), and 0.5 M 4-*tert*-butylpyridine (TBP) dissolved in acetonitrile.

Table 2
Detailed photovoltaic parameters of organic dyes (**S1**–**S4**) measured at an irradiance of 100 mW/cm^2 AM 1.5 G sunlight

Cell	V_{OC} (V)	J_{SC} (mA/cm^2)	FF	η (%)	τ_R (ms)[a]
S1	0.59	9.83	0.61	3.52	0.66
S2	0.61	12.27	0.63	4.73	0.43
S3	0.58	9.80	0.65	3.70	0.46
S4	0.50	3.83	0.65	1.24	0.26
N719	0.72	15.12	0.66	7.19	1.60

[a] τ_R: electron lifetime from the photovoltage measurement.

In order to investigate the extent of charge recombination between the oxidized dye and the redox couple, the recombination lifetime of photoinjected electrons with oxidized dyes was measured by transient photovoltage at open circuit with the presence of LiI (0.5 M) in acetonitrile. The average electron lifetime was estimated approximately by fitting a decay of the open circuit voltage transient with $\exp(-t/\tau_R)$, where t is time and τ_R is an average time constant before recombination. As shown in Fig. 7 and listed the fitting data in Table 2, the higher HOMO level of **S4** leads to a slower regeneration of the oxidized sensitizer with I^- and thus a faster recombination of photoinjected electrons.[40] Therefore, the photocurrent of **S4** is the lowest value among other dyes. The strong and bathochromic absorption of **S2** when compared with **S1** resulted in the high monochromic quantum efficiency and photocurrent. The longer electron lifetime of **S1** caused the higher monochromic quantum efficiency in the range of 350–550 nm than **S3**. Thus, the similar photocurrents of **S1** and **S3** were obtained.

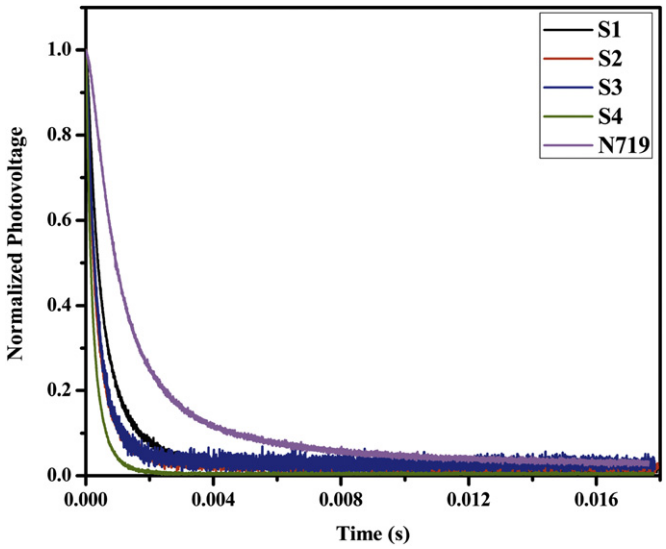

Fig. 7. Normalized electron lifetime of **S1**–**S4** and N719 dye as a function of extracted charge under open circuit condition with the presence of LiI electrolyte (0.5 M) in acetonitrile solutions.

To envisage the effects of co-adsorbent on the photovoltaic performance, **S2** and **S3** dyes were subjected to the studies of nanocrystalline TiO_2-based DSSCs using 10 mM of CDCA as a co-adsorbent during the sensitization processes. The IPCE and J–V curves of DSSCs bearing **S2** and **S3** dyes (with and without CDCA) are shown in Figs. 8a and b, respectively, and the detailed data are listed in Table 3. Regardless of the negligible improvement (2.1%) of efficiency in **S2**, the DSSC bearing **S3** dye showed a significant improvement (16.5%) in its PCE value, where the co-adsorption of CDCA prevented the dye aggregation and resulted in a more efficient electron injection from the excited dye to the conduction band of TiO_2, and thus to induce a significant improvement in J_{SC} value. Besides, there was considerable improvement in IPCE curve of **S3** dye (see Fig. 8a), which agreed well with its J_{SC} value (see Table 3). However, almost no change in η value of **S2** dye could be reasoned as the decrease of dye adsorption (without CDCA 2.91×10^{-7}, with CDCA 2.52×10^{-7} mol/cm^2) due to the use of CDCA[23,38] (see Table S1 of the Supplementary data) canceled with its enhanced electron injection from the excited dye to the conduction band of TiO_2. In general, it can be concluded that the applications of co-adsorbents enhance the electron injections from the oxidized dyes to the conduction bands of TiO_2 by suppressing the aggregations; on the other hand, the co-adsorbents decrease the net light harvesting by reducing the net dye adsorptions on the TiO_2 surfaces.

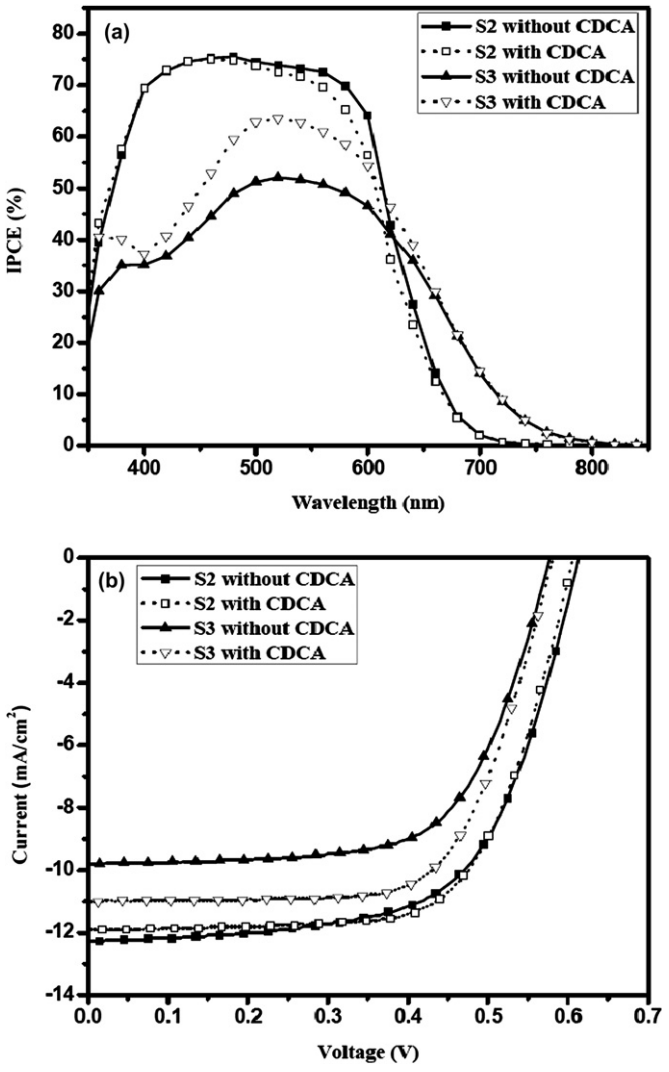

Fig. 8. (a) IPCE (b) J–V curves, of DSSCs based on **S2**–**S3** dyes(with and without CDCA) under illumination of simulated solar light (AM 1.5, 100 mW/cm^2). The electrode used was 0.5 M lithium iodide (LiI), 0.05 M iodine (I_2), and 0.5 M 4-*tert*-butylpyridine (TBP).

Table 3
Detailed photovoltaic parameters of organic dyes (**S2** and **S3**) with and without addition of CDCA during the sensitization process[a]

Dye	CDCA (mM)	V_{OC} (V)	J_{SC} (mA/cm^2)	FF	η (%)	Efficiency improvement
S2	0	0.61	12.27	0.63	4.73	2.1%
	10	0.61	11.91	0.66	4.83	
S3	0	0.58	9.80	0.65	3.70	16.5%
	10	0.58	11.01	0.67	4.31	

[a] Measured at an irradiance of 100 mW/cm^2 AM 1.5 G sunlight.

3. Conclusion

In summary, four novel A–D–A configured dyes (**S1**–**S4**) employing two different electron donating cores, such as the fluorene (**S1**–**S2**) and DTP (**S3**–**S4**) units, and two symmetrical anchoring cyanoacrylic acid (acceptor) termini linked via various numbers of thiophene units were synthesized and studied for their applications in DSSCs. In this A–D–A configuration, **S2** dye (containing electron donating fluorene units) showed the highest molar extinction coefficient, as a result it produced the highest PCE value (η=4.83%) with V_{OC}=0.61 V, J_{SC}=11.91 mA/cm^2, and FF=0.66 under standard AM 1.5 sunlight with a IPCE plateau of 76%. Besides, the

highly conjugated electron donating DTP moiety in **S3**–**S4** for the molecular design of DSSC dyes was first developed in this study. The symmetrical **S3** dye (containing an electron donating DTP core) showed an effective η=4.31%, with J_{SC}=11.01 mA/cm^2, V_{OC}=0.58 V, and FF=0.67. However, due to the high aggregation of dye molecules on TiO_2 surface and the short lifetime of the excited dyes, the DTP-based **S4** dye showed poor performance, which accelerated the charge recombination so as to decrease the photocurrent.

4. Experimental section

4.1. Materials

Chemicals and solvents were reagent grades and purchased from Aldrich, ACROS, TCI, Strem, Fluka, and Lancaster Chemical Co. THF (tetrahydrofuran) and DCM (dichloromethane) were distilled over sodium/benzophenone and calcium hydride, respectively, and freshly distilled before use. Tetra-*n*-butylammonium hexafluorophosphate ($TBAPF_6$) was recrystallized twice from absolute ethanol and further dried for two days under vacuum. *N*-Bromosuccinimide was recrystallized from distilled water and dried under vacuum. The other chemicals were used without further purification. The synthetic routes and detailed procedures of **S1**–**S4** dyes are shown in Scheme 1. 3,3′-Dibromo-2,2′-bithiophene (**4**),[36] 2,2′-(9,9-dihexyl-9*H*-fluorene-2,7-diyl)bis(4,4,5,5-tetramethyl-1,3,2-dioxaborolane) (**9**), and **7a**–**c**[41] were synthesized by the reported procedures. Intermediates **8a**–**b** and **10a**–**b** were synthesized by similar Suzuki coupling reaction and also **S1**–**S4** were synthesized by alike Knoevenagel reaction, where two examples of the detailed synthetic procedures for **8a** (Suzuki coupling reaction) and **S1** (Knoevenagel reaction) are described. In addition, the synthetic procedures of the other intermediates will be described as well. The chemical structures for all products were confirmed by ^{1}H and ^{13}C NMR spectroscopy, mass spectra (FAB), and elemental analyses. The ^{1}H NMR spectra of intermediate compounds **6**, **8a**, **8b**, **10a**, and **10b** (Figs. S2–S6) and both ^{1}H and ^{13}C NMR spectra of **S1**–**S4** dyes (Figs. S7–S14) are shown in the Supplementary data.

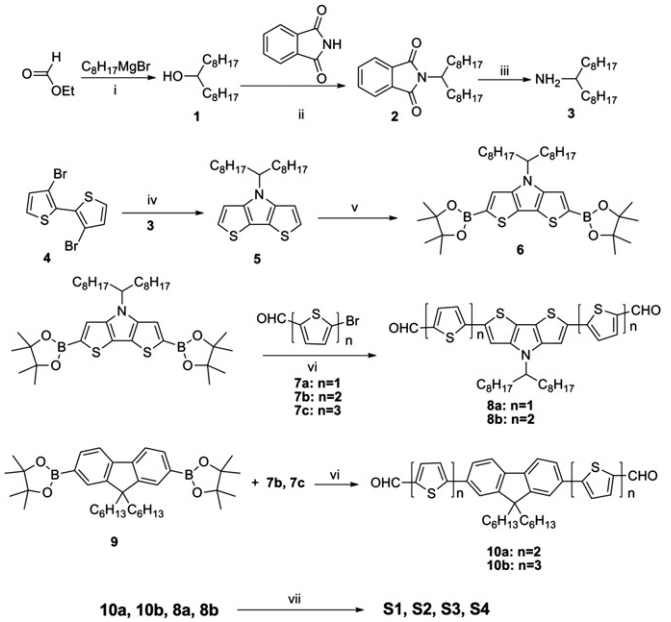

Scheme 1. Synthetic Routes of Dyes (**S1**–**S4**). (i) THF (ii) PPh_3, DIAD, Et_2O, room temperature (rt). (iii) (1) Hydrazine monohydrate, absolute ethanol, reflux; (2) 5.0 M HCl, reflux. (iv) Pd_2dba_3, BINAP, NaOtBu, toluene, 110 °C. (v) (1) *n*-BuLi, THF, −78 °C to rt; (2) 2-Isopropoxy-4,4,5,5-tetramethyl-[1,3,2] dioxaborolane, −78 °C to rt. (vi) Pd $(PPh_3)_4$, K_2CO_3, toluene/EtOH (3:1), 90 °C. (vii) $CNCH_2COOH$, NH_4OAc, CH_3COOH, 120 °C.

4.2. Synthesis

*4.2.1. Heptadecane-9-ol (**1**).* A solution of ethyl formate (10 g, 135 mmol) in dry THF (80 mL) was added dropwise to a fresh solution of octyl magnesium bromide, which was prepared from 1-bromooctane (58 g, 300 mmol) and magnesium (8.15 g, 340 mmol) in 150 mL dry THF. After then, the reaction mixture was stirred overnight at room temperature. Next, the reaction mixture was quenched by the addition of MeOH, followed by saturated aqueous NH_4Cl. The crude compound was extracted three times with ethyl acetate. The combined organic fractions were washed with brine and dried over $MgSO_4$. After removal of the solvent, the residue was purified by recrystalization from acetonitrile to afford heptadecane-9-ol (**1**) as white solids (30.91 g, 89.3%). ^{1}H NMR (300 MHz, $CDCl_3$), δ (ppm): 3.58 (m, 1H), 1.43–1.25 (m, 29H), 0.88 (t, *J*=6.6 Hz, 6H).

*4.2.2. 2-(Heptadecan-9-yl)isoindoline-1,3-dione (**2**).* A solution of **1** (10 g, 39 mmol), triphenylphosphine (10.22 g, 39 mmol), and phthalimide (5.74 g, 39 mmol) in dry diethyl ether (60 mL) was purged with N_2, and a solution of DIAD (7.70 mL, 39 mmol) in dry diethyl ether (30 mL) was added slowly. After stirring overnight, the precipitate was filtered off, and then washed thoroughly with diethyl ether. After removal of the solvent by rotary evaporator, the crude product was purified by column chromatography (silica) using hexane/dichloromethane (9:1) as an eluent to give a viscous and colorless oil (10.85 g, 72.2%). ^{1}H NMR (300 MHz, $CDCl_3$), δ (ppm): 7.82 (dd, *J*=3.3, 5.7 Hz, 2H), 7.70 (dd, *J*=3.0, 5.4 Hz, 2H), 4.21–4.14 (m, 1H), 2.10–1.99 (m, 2H), 1.78–1.64 (m, 2H), 1.25–1.26 (m, 24H), 0.84 (t, *J*=6.3 Hz, 6H).

*4.2.3. Heptadecan-9-amine (**3**).* A solution of **2** (15 g, 38.90 mmol) in absolute ethanol (200 mL) was purged with N2, and then hydrazine monohydrate (5.55 mL, 116.7 mmol) was added. The mixture was heated to reflux overnight (about 12 h). Subsequently, 12 mL of HCl solution (5 M) was added, and the mixture was refluxed for an additional 15 min and then cooled. The precipitate was filtered off and washed with water. Ethanol was removed from the filtrate by rotary evaporator, and NaOH solution (2 M) was added to make the solution alkaline (pH=10–11). The crude compound was extracted three times with ethyl acetate. The combined organic layers were washed with brine and dried over MgSO4, and the solvents were removed by rotary evaporator to get a colorless oil (6.07 g, 61.1%). ^{1}H NMR (300 MHz, $CDCl_3$), δ (ppm): 2.66 (m, 1H), 1.38–1.26 (m, 30H), 0.87 (t, *J*=6.3 Hz, 6H).

*4.2.4. 4-(Heptadecan-9-yl)-4H-dithieno[3,2-b:2′,3′-d]pyrrole (**5**).* Compound **4** (3 g, 9.3 mmol), *t*-BuONa (2.22 g, 23.10 mmol), Pd_2dba_3 (0.212 g, 0.231 mmol), and BINAP (0.575 g, 0.924 mmol) were dissolved in dry toluene (20 mL). The solution was purged with N_2 for 30 min. Heptadecan-9-amine (3) (2.84 g, 11.09 mmol) was added via a syringe and the mixture was stirred at 110 °C under N2 atmosphere for 12 h. After cooling, water was added and extracted twice with diethyl ether. The combined organic layers were dried over MgSO4, and the solvents were removed by rotary evaporator. The crude product was purified by column chromatography (silica) using hexane as an eluent to give a white solid (3.1 g, 80.30%). ^{1}H NMR (300 MHz, $CDCl_3$), δ (ppm): 7.10 (d, *J*=5.1 Hz, 2H), 7.01 (d, *J*=5.1 Hz, 2H), 4.24–4.18 (m, 1H), 2.06–1.97 (m, 2H), 1.87–1.78 (m, 2H), 1.61 (m, 24H), 0.85 (t, *J*=6.9 Hz, 6H).

*4.2.5. 4-(Heptadecan-9-yl)-2,6-bis(4,4,5,5-tetramethyl-1,3,2-dioxaborolan-2-yl)-4H-dithieno[3,2-b:2′,3′-d]pyrrole (**6**).* Compound **5** (1 g, 2.4 mmol) was dissolved in 50 mL of dry THF and the solution was cooled down to −78 °C under nitrogen protection, then 2.4 mL of *n*-BuLi (2.5 M in Hexane, 5.98 mmol) was added. The solution was warmed up to room temperature for 30 min and cooled again

to −78 °C. 2-Isopropoxy-4,4,5,5-tetramethyl-[1,3,2] dioxaborolane (1.37 mL, 6.7 mmol) was rapidly injected into the solution by a syringe, and the resulting mixture was stirred at −78 °C for 1 h, and followed by reacting overnight at room temperature. The resulting mixture was quenched with H_2O and extracted with dichloromethane. The dichloromethane extracts were washed with saturated brine and dried with $MgSO_4$. The solvent was removed by rotary evaporator and the product was further purified by column chromatography (silica) using a mixture of hexane and dichloromethane (4:1) as an eluent to yield a white solid (0.72 g, 45%). Mp: 147–149 °C. ^{1}H NMR (300 MHz, $CDCl_3$), δ (ppm): 7.50 (s, 2H), 4.25–4.16(m, 1H), 2.08–1.86 (m, 2H), 1.86–1.76 (m, 2H), 1.37 (s, 24H), 1.14 (m, 24H), 0.84 (t, J=6.9 Hz, 6H). ^{13}C NMR (75 MHz, $CDCl_3$), δ (ppm): 147.8, 126.0, 120.7, 121.5, 84.3, 60.3, 35.2, 31.7, 31.5, 26.6, 25.0, 22.6, 14.2. MS (FAB): m/z [M^+] 670; calcd m/z [M^+] 669.42.

*4.2.6. 5,5′-(4-(Heptadecan-9-yl)-4H-dithieno[3,2-b:2′,3′-d]pyrrole-2,6-diyl) dithiophene-2-carbaldehyde (**8a**).* Mixture of compounds **6** (0.3 g, 0.46 mmol), **7a** (0.197 g, 1.03 mmol), and K_2CO_3 (0.161 g, 1.16 mmol) were dissolved in 20 mL of toluene/ethanol (3:1) and degassed for 10 min, which was followed by the addition of 20 mg Pd $(PPh_3)_4$ as a catalyst. The resulting mixture was stirred under reflux for 36 h. The solvent was removed under vacuum and extracted with dichloromethane and washed with water followed by a little brine. The organic phase was dried with anhydrous $MgSO_4$, and the solvent was removed by rotary evaporator. Afterward, the crude compound was purified by column chromatography (silica) using a mixture of hexane and dichloromethane (1:1) as an eluent. The obtained product was recrystallized from ethanol to yield an orange color solid (210 mg, 70%). Mp: 128–130 °C. ^{1}H NMR (300 MHz, DMSO-d_6), δ (ppm): 9.85 (s, 2H), 7.96 (d, J=3.9 Hz, 2H), 7.91 (s, 2H), 7.53 (d, J=3.9 Hz, 2H), 4.49–4.44 (m, 1H), 2.06–2.03 (m, 2H), 1.83–1.79 (m, 2H), 1.06 (m, 24H), 0.71 (t, J=6.9 Hz, 6H). ^{13}C NMR (75 MHz, DMSO-d_6), δ (ppm): 182.5, 148.2, 146.6, 142.1, 134.5, 133.9, 124.9, 59.6, 34.4, 31.7, 29.3, 29.0, 26.4, 22.6, 14.4. MS (FAB): m/z [M^+] 638; calcd m/z [M^+] 637.22.

*4.2.7. 5′,5″-(4-(Heptadecan-9-yl)-4H-dithieno[3,2-b:2′,3′-d]pyrrole-2,6-diyl)di-2′,2″-bithiophene-5-carbaldehyde (**8b**).* Compound **8b** was synthesized by the same procedure as compound **8a**, afforded an orange solid in 69.5% yield. Mp: 135–137 °C. ^{1}H NMR (300 MHz, DMSO-d_6), δ (ppm): 9.86 (s, 2H), 7.98 (d, J=3.9 Hz, 2H), 7.70 (s, 2H), 7.55 (d, J=3.9 Hz, 2H), 7.51 (d, J=3.9 Hz, 2H), 7.35 (d, J=3.9 Hz, 2H), 4.44 (m, 1H), 2.03 (m, 2H), 1.80 (m, 2H), 1.13–0.95 (m, 24H), 0.72 (t, J=6.9 Hz, 6H). ^{13}C NMR (75 MHz, DMSO-d_6), δ (ppm): 182.7, 146.6, 146.0, 142.1, 140.0, 134.2, 133.3, 128.7, 125.1, 59.8, 34.4, 31.8, 29.4, 29.2, 26.4, 22.6, 14.4. MS (FAB): m/z [M^+] 802; calcd m/z [M^+] 801.19.

*4.2.8. 5′,5″-(9,9-Dihexyl-9H-fluorene-2,7-diyl)di-2,2′-bithiophene-5′-carbaldehyde (**10a**).* Compound **10a** was synthesized by the same procedure as compound **8a**, afforded a yellow solid in 78.2% yield. Mp: 143–145 °C. ^{1}H NMR (300 MHz, $CDCl_3$), δ (ppm): 9.89 (s, 2H), 7.73–7.69 (m, 4H), 7.62 (dd, J=1.5, 7.8 Hz, 2H), 7.56 (s, 2H), 7.39–7.35 (m, 4H), 7.30 (d, J=3.9 Hz, 2H), 2.07–2.01(m, 4H), 1.14–1.06 (m, 12H), 0.75 (t, J=6.6 Hz, 6H), 0.69 (m, 4H). ^{13}C NMR (75 MHz, $CDCl_3$), δ (ppm): 182.6, 152.21, 147.4, 147.0, 141.76, 140.0, 137.6, 135.1, 132.8, 127.4, 125.2, 124.3, 124.2, 120.7, 120.2, 55.6, 40.6, 31.7, 29.85, 23.0, 22.8, 14.2. MS (FAB): m/z [M^+] 719; calcd m/z [M^+] 718.21.

*4.2.9. 5′,5″-(9,9-Dihexyl-9H-fluorene-2,7-diyl)-di-2,2′:5′,2″-terthiophene-5″-carbaldehyde (**10b**).* Compound **10b** was synthesized by the same procedure as compound **8a**, afforded a reddish yellow solid in 75.0% yield. Mp: 184–186 °C. ^{1}H NMR (300 MHz, $CDCl_3$), δ (ppm): 9.87 (s, 2H), 7.71–7.68 (m, 4H), 7.60 (dd, J=1.8, 8.1 Hz, 2H), 7.56 (s, 2H), 7.33 (d, J=3.9 Hz, 2H), 7.31 (d, J=3.9 Hz, 2H) 7.26–7.23 (m, 4H), 7.18 (d, J=3.9 Hz, 2H), 2.06–2.01(m, 4H), 1.15–1.07 (m, 12H), 0.76 (t, J=6.6 Hz, 6H), 0.69 (m, 4H). ^{13}C NMR (75 MHz, $CDCl_3$), δ (ppm): 182.6, 152.1, 147.0, 145.2, 141.8, 140.7, 139.5, 137.6, 135.6, 134.6, 132.9, 127.3, 125.7, 125.0, 124.7, 124.2, 124.0, 120.5, 120.0, 55.6, 40.6, 31.68, 29.9, 23.0, 22.8, 14.2. MS (FAB): m/z [M^+] 883; calcd m/z [M^+] 882.18.

*4.2.10. (2E,2′E)-3,3′-(5′,5″-(9,9-Dihexyl-9H-fluorene-2,7-diyl)bis(2,2′-bithiophene-5′,5-diyl))bis(2-cyanoacrylic acid) (**S1**).* Acetic acid (40 mL) was added to a flask containing a mixture of compound **10a** (400 mg, 0.56 mmol), ammonium acetate (170 mg, 2.25 mmol), and cyanoacetic acid (236 mg, 2.35 mmol). The mixture was refluxed for 36 h and allowed to cool to room temperature. The resulting solid was filtered and washed with excess of distilled water, followed by dichloromethane to give a dark brown solid (390 mg, 82.4%). Mp: 287–289 °C. ^{1}H NMR (300 MHz, DMSO-d_6), δ (ppm): 8.49 (s, 2H), 7.98 (d, J=4.5 Hz, 2H), 7.87–7.81 (m, 4H), 7.70 (dd, J=3.3 Hz, J=9.9 Hz, 6H), 7.62 (d, J=3.9 Hz, 2H), 2.06 (m, 4H), 1.03–0.96 (m, 12H), 0.66 (t, J=6.3 Hz, 6H), 0.51 (m, 4H). ^{13}C NMR (75 MHz, DMSO-d_6), δ (ppm): 164.3, 152.3, 147.0, 146.6, 146.3, 142.3, 141.0, 134.6, 132.6, 129.1, 126.2, 125.6, 125.4, 121.5, 120.4, 117.3, 98.7, 55.8, 31.5, 29.5, 24.1, 22.6, 14.5. MS (FAB): m/z [M^+] 853; calcd m/z [M^+] 852.22. Anal. Calcd for $C_{49}H_{44}N_2O_4S_4$: C, 68.98; H, 5.20; N, 3.28. Found: C, 68.62; H, 5.49; N, 3.26.

*4.2.11. 5′,5″-(9,9-Dihexyl-9H-fluorene-2,7-diyl)-di-[2,2′:5′,2″-terthiophene-5″-(2-cyanoacrylic acid)] (**S2**).* Compound **S2** dye was synthesized by the same procedure as **S1**, afforded dark brown solid in 82.0% yield. Mp: 302–304 °C. ^{1}H NMR (300 MHz, DMSO-d_6), δ (ppm): 8.47 (s, 2H), 7.97 (d, J=4.2 Hz, 2H), 7.83–7.76 (m, 4H), 7.63–7.58 (m, 8H), 7.49 (d, J=3.6 Hz, 2H), 7.42 (d, J=3.9 Hz, 2H), 2.06 (m, 4H), 1.00–0.95 (m, 12H), 0.65 (t, J=6.3 Hz, 6H), 0.53 (m, 4H). ^{13}C NMR (75 MHz, DMSO-d_6), δ (ppm): 164.3, 152.2, 146.9, 145.8, 144.6, 142.1, 140.7, 139.0, 135.1, 134.7, 134.2, 132.8, 128.8, 127.1, 126.1, 125.1, 125.0, 121.3, 120.1, 117.2, 98.1, 55.1, 31.0, 29.1, 24.1, 22.1, 14.4. MS (FAB): m/z [M^+] 1017; calcd m/z [M^+] 1016.19. Anal. Calcd for $C_{57}H_{48}N_2O_4S_6$: C, 67.29; H, 4.76; N, 2.75. Found: C, 66.61; H, 5.02; N, 2.85.

*4.2.12. (2E,2′E)-3,3′-(5,5′-(4-(Heptadecan-9-yl)-4H-dithieno[3,2-b:2′,3′-d]pyrrole-2,6-diyl)bis(thiophene-5,2-diyl))bis(2-cyanoacrylic acid) (**S3**).* Compound **S3** dye was synthesized by the same procedure as **S1**, afforded dark brown solid in 89.6% yield. Mp: 281–283 °C. ^{1}H NMR (300 MHz, DMSO-d_6), δ (ppm): 8.44 (s, 2H), 7.94 (d, J=4.5 Hz, 2H), 7.90 (s, 2H), 7.58 (d, J=3.9 Hz, 2H), 4.49 (m, 1H), 2.07–2.03 (m, 2H), 1.78–1.74 (m, 2H), 1.04 (m, 24H) 0.71 (t, J=6.9 Hz, 6H). ^{13}C NMR (75 MHz, DMSO-d_6), δ (ppm) 164.5, 148.4, 146.8, 142.3, 134.6, 134.1, 125.0, 117.4, 116.7, 112.4, 97.9, 59.8, 34.5, 31.9, 29.4, 29.2, 26.5, 22.7, 14.5. MS (FAB): m/z [M^+] 772; calcd m/z [M^+] 771.23. Anal. Calcd for $C_{41}H_{45}N_3O_4S_4$: C, 63.78; H, 5.87; N, 5.44. Found: C, 63.34; H, 5.80; N, 5.30.

*4.2.13. (2E,2′E)-3,3′-(5′,5″-(4-(Heptadecan-9-yl)-4H-dithieno[3,2-b:2′,3′-d]pyrrole-2,6-diyl)bis(2′,2″-bithiophene-5′,5′-diyl))bis(2-cyanoacrylic acid) (**S4**).* Compound **S4** dye was synthesized by the same procedure as **S1**, afforded dark brown solid in 88.2% yield. Mp: 292–294 °C. ^{1}H NMR (300 MHz, DMSO-d_6), δ (ppm): 8.42 (s, 2H), 7.92 (d, J=4.2 Hz, 2H), 7.68 (s, 2H), 7.51–7.46 (m, 4H), 7.29 (d, J=3.6 Hz, 2H), 4.39 (m, 1H), 2.01 (m, 2H), 1.75 (m, 2H), 1.11–0.91 (m, 24H) 0.70 (t, J=6.6 Hz, 6H). ^{13}C NMR (75 MHz, DMSO-d_6), δ (ppm): 164.3, 146.8, 146.1, 142.3, 140.9, 134.4, 134.2, 133.4, 128.8, 125.3, 117.3, 110.8, 98.5, 59.9, 34.6, 31.9, 29.5, 29.2, 26.5, 22.7, 14.5. MS (FAB): m/z [M^+] 935; calcd m/z [M^+] 935.20. Anal. Calcd for $C_{49}H_{49}N_3O_4S_6$: C, 62.85; H, 5.27; N, 4.49. Found: C, 62.62; H, 5.58; N, 4.78.

4.3. Measurement and characterizations

^{1}H NMR spectra were recorded on a Varian unity 300 MHz spectrometer using DMSO-d_6 and $CHCl_3$-d as solvents. Elemental analyses were performed on a HERAEUS CHN-OS RAPID elemental

analyzer. UV–vis absorption spectra were recorded in dilute THF solutions (10^{-5} M) on an HP G1103A spectrophotometer, and photoluminescence (PL) spectra were obtained on a Hitachi F-4500 spectrophotometer. Cyclic voltammetry (CV) measurements were performed using a BAS 100 electrochemical analyzer with a standard three-electrode electrochemical cell in a 0.1 M tetrabutylammonium hexafluorophosphate ($TBAPF_6$) solution (in THF) at room temperature with a scanning rate of 100 mV/s. During the CV measurements, the solutions were purged with nitrogen for 30 s. In each case, a carbon coating rod as the working electrode, a platinum wire as the counter electrode, and a silver wire as the quasi-reference electrode were used, and Ag/AgCl (3 M KCl) electrode was served as the reference electrode for all potentials quoted herein. The redox couple of ferrocene/ferrocenium ion (Fc/Fc^+) was used as an external standard. The corresponding HOMO and LUMO levels were calculated from the onset oxidation potential ($E_{ox/onset}$) and UV–vis absorption edge (Eg^{opt}), respectively.

4.3.1. TiO_2 paste preparation. The preparation of TiO_2 precursor and the electrode fabrication were carried out based on previous report.[42] with an autoclaved temperature of 240 °C. The precursor solution was made according to the following procedure: 430 mL of 0.1 M nitric acid solution under vigorous stirring was slowly combined with 72 mL $Ti(C_3H_7O)_4$ to form a mixture. After the hydrolysis, the mixture was heated at 85 °C in a water bath and stirred vigorously for 8 h in order to achieve the peptization. When the mixture was cooled down to room temperature, the resultant colloid was filtered, and the filtrate was then heated in an autoclave at a temperature of 240 °C for 12 h to grow the TiO_2 particles. When the colloid was cooled to room temperature, it was ultrasonically vibrated for 10 min. The TiO_2 colloid was concentrated to 13 wt %, followed by the addition of 30 wt % (with respect to TiO_2 weight) of poly (ethylene glycol) (PEG, MW=20,000 g/mol) to prevent the film from cracking while drying.

4.3.2. Device fabrication. The TiO_2 paste was then deposited on an FTO glass substrate by the glass rod method with a dimension of 0.5×0.5 cm^2. The polyester tape (3 M) was used as an adhesive on two edges of an FTO glass. The tape was removed after the TiO_2 paste was spread on the FTO by a glass rod and the TiO_2 paste was dried in the air at room temperature for 1 h. The TiO_2-coated FTO was heated to 500 °C at a heating rate of 10 °C/min and maintained for 30 min before cooled to room temperature. After repeating the same procedure described above to control the thickness of a TiO_2 film, the final coating was carried out with TiO_2 pastes containing different sizes (300 nm and 20 nm with weight percentages of 30 and 70, respectively) of light scattering TiO_2 particles and then heated to 500 °C. The thicknesses of TiO_2 films were measured by a profilometer (Dektak3, Veeco/Sloan Instruments, Inc.). The adsorbed density of each dye was calculated from the concentration difference of each solution before and after TiO_2 film immersion. The TiO_2 electrode with a geometric area of 0.25 cm^2 was immersed in a acetonitrile/*tert*-butanol mixture (volume ratio 1:1) containing 3×10^{-4} M *cis*-di(thiocyanato)bis(2,2′-bipyridyl-4,4′-dicarboxylato) ruthenium(II) bis(tetrabutylammonium) (N719, Solaronix SA) or in the THF solutions containing 3×10^{-4} M organic sensitizers for overnight. A thermally platinized FTO was used as a counter electrode and was controlled to have an active area of 0.36 cm^2 by adhered polyester tape with a thickness of 60 μm. After rinsing with CH_3CN or THF, the photoanode was placed on top of the counter electrode and tightly clipping them together to form a cell. Electrolyte was then injected into the space and then sealing the cell with the Torr Seal cement (Varian, Inc.). The electrolyte was composed of 0.5 M lithium iodide (LiI), 0.05 M iodine (I_2), and 0.5 M 4-*tert*-butylpyridine (TBP) dissolved in acetonitrile. The photovoltage transients of assembled devices were recorded with a digital oscilloscope (LeCroy, WaveSurfer 24Xs). Pulsed laser excitation was applied by a Q-switched Nd:YAG laser (Continuum, model Minilite II) with 1 Hz repetition rate at 532 nm and a 5 ns pulse width at half-height. The beam size was slightly larger than 0.5×0.5 cm^2 to cover the area of the device. The photovoltage of each device was adjusted by incident pulse energy to be 40 mV.

4.3.3. Device measurements. A 0.6×0.6 cm^2 cardboard mask was clipped onto the device to constrain the illumination area. The photoelectrochemical characterizations on the solar cells were carried out by using an Oriel Class A solar simulator (Oriel 91195A, Newport Corp.). Photocurrent–voltage characteristics of the DSSCs were recorded with a potentiostat/galvanostat (CHI650B, CH Instruments, Inc.) at a light intensity of 1.0 sun calibrated by an Oriel reference solar cell (Oriel 91150, Newport Corp.). The monochromatic quantum efficiency was recorded through a monochromator (Oriel 74100, Newport Corp.) at short circuit condition. The intensity of each wavelength was in the range of 1–3 mW/cm^2. The photovoltage transients of assembled devices were recorded with a digital oscilloscope (LeCroy, WaveSurfer 24Xs). Pulsed laser excitation was applied by a Q-switched Nd:YAG laser (Continuum, model Minilite II) with 1 Hz repetition rate at 532 nm and a 5 ns pulse width at half-height. The beam size was slightly larger than 0.5×0.5 cm^2 to cover the area of the device. The photovoltage of each device was adjusted by incident pulse energy to be 50 mV. The average electron lifetime can be estimated approximately by fitting a decay of the open circuit voltage transient with $\exp(-t/\tau_R)$, where t is time and τ_R is an average time constant before recombination.

4.3.4. Quantum chemistry computation. The predicted structures of the molecules were optimized by using B3LYP hybrid functional, and 6-31G* basis sets. For each of the molecules, a number of conformational isomers were examined and the one with the lowest energy was used. For the excited states, we have employed the time-dependent density functional theory (TD-DFT) with the B3LYP functional. The lowest 33 singlet–singlet excited states were calculated using TDDFT (up to an energy of ca. 250 nm). All of the analyses were performed under Gaussian 03 (G03) (revision E.01) program package[43] by using density functional theory (DFT). The simulated spectra with the oscillator strength (f) values were obtained with the program GaussSum 2.1.2.

Acknowledgements

We are grateful to the National Center for High-performance computing for computer time and facilities. The financial supports of this project provided by the National Science Council of Taiwan (ROC) through NSC 97-2113-M-009-006-MY2, National Chiao Tung University through 97W807, and Energy and Environmental Laboratories (charged by Dr. Chang-Chung Yang) in Industrial Technology Research Institute (ITRI) are acknowledged.

Supplementary data

Supplementary data associated with this article can be found in online version at doi:10.1016/j.tet.2010.11.044. These data include MOL files and InChIKeys of the most important compounds described in this article.

References and notes

1. (a) Gaudiana, R. *J. Phys. Chem. Lett.* **2010**, *1*, 1288; (b) Hagfeldt, A.; Grätzel, M. *Chem. Rev.* **1995**, *95*, 49.
2. O'Regan, B.; Grätzel, M. *Nature* **1991**, *353*, 737.
3. Grätzel, M. *Nature* **2001**, *414*, 338.
4. (a) Nazeeruddin, M. K.; Kay, A.; Rodicio, I.; Humpbry-Baker, R.; Miiller, E.; Liska, P.; Vlachopoulos, N.; Grätzel, M. *J. Am. Chem. Soc.* **1993**, *115*, 6382; (b)

Staniszewski, A.; Ardo, S.; Sun, Y.; Castellano, E. N.; Meyer, G. J. *J. Am. Chem. Soc.* **2008**, *130*, 11586; (c) Sauvage, F.; Fischer, M. K. R.; Mishra, A.; Zakeeruddin, S. M.; Nazeeruddin, M. K.; Bäuerle, P.; Grätzel, M. *ChemSusChem* **2009**, *2*, 761.
5. (a) Nazeeruddin, M. K.; Zakeeruddin, S. M.; Humphry-Baker, R.; Jirousek, M.; Liska, P.; Vlachopoulos, N.; Shklover, V.; Fischer, C.-H.; Grätzel, M. *Inorg. Chem.* **1999**, *38*, 6298; (b) Schmidt-Mende, L.; Kroeze, J. E.; Durrant, J. R.; Nazeeruddin, M. K.; Grätzel, M. *Nano Lett.* **2005**, *5*, 1315.
6. Chen, C.-Y.; Chen, J.-G.; Wu, S.-J.; Li, J.-Y.; Wu, C.-G.; Ho, K.-C. *Angew. Chem., Int. Ed.* **2008**, *47*, 7342.
7. Abbotto, A.; Barolo, C.; Bellotto, L.; De Angelis, F.; Grätzel, M.; Manfredi, N.; Marinzi, C.; Fantacci, S.; Yum, J.-H.; Nazeeruddin, M. K. *Chem. Commun.* **2008**, 5318.
8. Yin, J.-F.; Chen, J.-G.; Lu, Z.-Z.; Ho, K.-C.; Lin, H.-C.; Lu, K.-L. *Chem. Mater.* **2010**, *22*, 4392.
9. Yin, J.-F.; Bhattacharya, D.; Hsu, Y.-C.; Tsai, C.-C.; Lu, K.-L.; Lin, H.-C.; Chen, J.-G.; Ho, K.-C. *J. Mater. Chem.* **2009**, *19*, 7036.
10. (a) Wang, Z.-S.; Cui, Y.; Dan-oh, Y.; Kasada, C.; Shinpo, A.; Hara, K. *J. Phys. Chem. C* **2007**, *111*, 7224; (b) Hara, K.; Sayama, K.; Ohga, Y.; Shinpo, A.; Suga, S.; Arakawa, H. *Chem. Commun.* **2001**, 569; (c) Hara, K.; Kurashige, M.; Danoh, Y.; Kasada, C.; Shinpo, A.; Suga, S.; Sayama, K.; Arakawa, H. *New J. Chem.* **2003**, *27*, 783.
11. Tanaka, H.; Takeichi, A.; Higuchi, K.; Motohiro, T.; Takata, M.; Hirota, N.; Nakajima, J.; Toyoda, T. *Sol. Energy Mater. Sol. Cells* **2009**, *93*, 1143.
12. Ito, S.; Zakeeruddin, S. M.; Humphry-Baker, R.; Liska, P.; Charvet, R.; Comte, P.; Nazeeruddin, M. K.; Péchy, P.; Takata, M.; Miura, H.; Uchida, S.; Grätzel, M. *Adv. Mater.* **2006**, *18*, 1202.
13. Tang, J.; Wu, W.; Hua, J.; Li, J.; Li, X.; Tian, H. *Energy Environ. Sci.* **2009**, *2*, 982.
14. Guo, M.; Diao, P.; Ren, Y.-J.; Meng, F.; Tian, H.; Cai, S.-M. *Sol. Energy Mater. Sol. Cells* **2005**, *88*, 23.
15. Sayama, K.; Tsukagoshi, S.; Mori, T.; Hara, K.; Ohga, Y.; Shinpou, A.; Abe, Y.; Suga, S.; Arakawa, H. *Sol. Energy Mater. Sol. Cells* **2003**, *80*, 47.
16. Shibano, Y.; Umeyama, T.; Matano, Y.; Imahori, H. *Org. Lett.* **2007**, *9*, 1971.
17. (a) Won, Y. S.; Yang, Y. S.; Kim, J. H.; Ryu, J.-H.; Kim, K. K.; Park, S. S. *Energy Fuels* **2010**, *24*, 3676; (b) Tan, S.; Zhai, J.; Fang, H.; Jiu, T.; Ge, J.; Li, Y.; Jiang, L.; Zhu, D. *Chem.—Eur. J.* **2005**, *11*, 6272.
18. Thomas, K. R. J.; Lin, J. T.; Hsu, Y.-C.; Ho, K.-C. *Chem. Commun.* **2005**, 4098.
19. (a) Chen, C.-H.; Hsu, Y.-C.; Chou, H.-H.; Thomas, K. R. J.; Lin, J. T.; Hsu, C.-P. *Chem.—Eur. J.* **2010**, *16*, 3184; (b) Baheti, A.; Tyagi, P.; Thomas, K. R. J.; Hsu, Y.-C.; Lin, J. T. *J. Phys. Chem. C* **2009**, *113*, 8541.
20. (a) Kim, S.; Choi, H.; Kim, D.; Song, K.; Kang, S. O.; Ko, J. *Tetrahedron* **2007**, *63*, 9206; (b) Choi, H.; Lee, J. K.; Song, K.; Kang, S. O.; Ko, J. *Tetrahedron* **2007**, *63*, 3115.
21. (a) Mishra, A.; Fischer, M. K. R.; Bäuerle, P. *Angew. Chem., Int. Ed.* **2009**, *48*, 2474; (b) Li, Y.-T.; Chen, C.-L.; Hsu, Y.-Y.; Hsu, H.-C.; Chi, Y.; Chen, B.-S.; Liu, W.-H.; Lai, C.-H.; Lin, T.-Y.; Chou, P.-T. *Tetrahedron* **2010**, *66*, 4223; (c) Zhang, L.; Liu, Y.; Wang, Z.; Liang, M.; Sun, Z.; Xue, S. *Tetrahedron* **2010**, *66*, 3318; (d) Hwang, S.; Lee, J. H.; Park, C.; Lee, H.; Kim, C.; Park, C.; Lee, M.-H.; Lee, W.; Park, J.; Kim, K.; Park, N.-G.; Kim, C. *Chem. Commun.* **2007**, 4887.
22. (a) Chen, H.; Huang, H.; Huang, X.; Clifford, J. N.; Forneli, A.; Palomares, E.; Zheng, X.; Zheng, L.; Wang, X.; Shen, P.; Zhao, B.; Tan, S. *J. Phys. Chem. C* **2010**, *114*, 3280; (b) Kim, D.; Kang, M. S.; Song, K.; Kang, S. O.; Ko, J. *Tetrahedron* **2008**, *63*, 10417.
23. Qu, S.; Wu, W.; Hua, J.; Kong, C.; Long, Y.; Tian, H. *J. Phys. Chem. C* **2010**, *114*, 1343.
24. (a) Im, H.; Kim, S.; Park, C.; Jang, S.-H.; Kim, C.-J.; Kim, K.; Park, N.-G.; Kim, C. *Chem. Commun.* **2010**, *46*, 1335; (b) Burke, A.; Schmidt-Mende, L.; Ito, S.; Grätzel, M. *Chem. Commun.* **2007**, 234; (c) Snaith, H. J. *Adv. Funct. Mater.* **2010**, *20*, 13; (d) Velusamy, M.; Thomas, K. R. J.; Lin, J. T.; Hsu, Y.-C.; Ho, K. C. *Org. Lett.* **2005**, *7*, 1899.
25. Park, S. S.; Won, Y. S.; Choi, Y. C.; Kim, J. H. *Energy & Fuels* **2009**, *23*, 3732.
26. Abbotto, A.; Manfredi, N.; Marinzi, C.; De Angelis, F.; Mosconi, E.; Yum, J.-H.; Xianxi, Z.; Nazeeruddin, M. K.; Grätzel, M. *Energy Environ. Sci.* **2009**, *2*, 1094.
27. Heredia, D.; Natera, J.; Gervaldo, M.; Otero, L.; Fungo, F.; Lin, C.-Y.; Wong, K.-T. *Org. Lett.* **2010**, *12*, 12.
28. Ogawa, K.; Rasmussen, S. C. *J. Org. Chem.* **2003**, *68*, 2921.
29. Mishara, S. P.; Palai, A. K.; Srivastava, R.; Kamalasanan, M. N.; Patri, M. *J. Polym. Sci., Part A: Polym. Chem.* **2009**, *47*, 6514.
30. (a) Zhou, E.; Nakamura, M.; Nishizawa, T.; Zhang, Y.; Wei, Q.; Tajima, K.; Yang, C.; Hashimoto, K. *Macromolecules* **2008**, *41*, 8302; (b) Yue, W.; Zhao, Y.; Shao, S.; Tian, H.; Xie, Z.; Geng, Y.; Wang, F. *J. Mater. Chem.* **2009**, *19*, 2199; (c) Zhou, E.; Yamakawa, S.; Tajima, K.; Yang, C.; Hashimoto, K. *Chem. Mater.* **2009**, *21*, 4055.
31. Liu, J.; Zhang, R.; Sauvé, G.; Kowalewski, T.; McCullough, R. D. *J. Am. Chem. Soc.* **2008**, *130*, 13167.
32. Sanchez-Diaz, A.; Martinez-Ferrero, E.; Palomares, E. *J. Mater. Chem.* **2009**, *19*, 5381.
33. Gonçalves, A. S.; Davolos, M. R.; Masaki, N.; Yanagida, S.; Mori, S.; Nogueira, A. F. *J. Appl. Phys.* **2009**, *106*, 064316.
34. Kopidakis, N.; Benkstein, K. D.; de Lagemaat, J. V.; Frank, A. J. *J. Phys. Chem. B* **2003**, *107*, 11307.
35. Yang, H.-Y.; Yen, Y.-S.; Hsu, Y.-C.; Chou, H.-H.; Lin, J. T. *Org. Lett.* **2010**, *12*, 16.
36. Wei, Y.; Yang, Y.; Yeh, J.-M. *Chem. Mater.* **1996**, *8*, 2659.
37. (a) Chen, K.-F.; Hsu, Y.-C.; Wu, Q.; Yeh, M.-C. P.; Sun, S.-S. *Org. Lett.* **2009**, *11*, 377; (b) Li, G.; Jiang, K. J.; Bao, P.; Li, Y.-F.; Li, S.-L.; Yang, L.-M. *New J. Chem.* **2009**, *33*, 868.
38. Fischer, M. K. R.; Wenger, S.; Wang, M.; Mishra, A.; Zakeeruddin, S. M.; Grätzel, M.; Bäuerle, P. *Chem. Mater.* **2010**, *22*, 1836.
39. Cao, Y.; Bai, Y.; Yu, Q.; Cheng, Y.; Liu, S.; Shi, D.; Gao, F.; Wang, P. *J. Phys. Chem. C* **2009**, *113*, 6290.
40. O'Regan, B. C.; Durrant, J. R. *J. Phys. Chem. B* **2006**, *110*, 8544.
41. Zhu, Y.; Rabindranath, A. R.; Beyerlein, T.; Tieke, B. *macromolecules* **2007**, *40*, 6981.
42. Huang, C. Y.; Hsu, Y.-C.; Chen, J.-G.; Suryanarayanan, V.; Lee, K. M.; Ho, K.-C. *Sol. Energy Mater. Sol. Cells* **2006**, *90*, 2391.
43. Pople, J. A. *Gaussian 03, Revision E.01*; Gaussian: Wallingford, CT, 2004.